analytical chemistry

Article

Cite This: *Anal. Chem.* 2019, 91, 7366−7372

pubs.acs.org/ac

Method for Determining Average Iron Content of Ferritin by Measuring its Optical Dispersion

Ruchi Gupta,*[,†] Nasser A. Alamrani,[‡] Gillian M. Greenway,[‡] Nicole Pamme,[‡] and Nicholas J. Goddard[§]

[†]School of Chemistry, University of Birmingham, Birmingham B15 2TT, U.K.

[‡]Department of Chemistry and Biochemistry, University of Hull, Hull HU6 7RX, U.K.

[§]Process Instruments (U.K.) Ltd., March Street, Burnley BB12 0BT, U.K.

Supporting Information

ABSTRACT: We report a method where the refractive index increments of an iron storage protein, ferritin, and apoferritin (ferritin minus iron) were measured over the wavelength range of 450−678 nm to determine the average iron content of the protein. The protein used in this study had ∼3375 iron atoms per molecule. The measurement of optical dispersion over the broad wavelength range was enabled by the use of mesoporous leaky waveguides (LWs) made of chitosan. We present a facile approach for fabricating mesoporous chitosan waveguides for improving the measurement sensitivity of macromolecules such as ferritin. Mesoporous materials allow macromolecules to diffuse into the waveguide, maximizing their interaction with the optical mode and thus increasing sensitivity by a factor of ∼9 in comparison to nonporous waveguides. The sensitivity was further improved and selectivity toward ferritin was achieved by the incorporation of antibodies in the waveguide. The method presented in this work is a significant advance over the state of the art method, the enzyme linked immunosorbent assay (ELISA) used in clinics, because it allows determining the average content of ferritin in a single step. The average iron content of ferritin is an important marker for conditions such as injury, inflammation, and infection. Thus, the approach presented here of measuring optical dispersion to determine the average iron content of ferritin has a significant potential to improve the point of care analysis of the protein for disease diagnosis and screening.

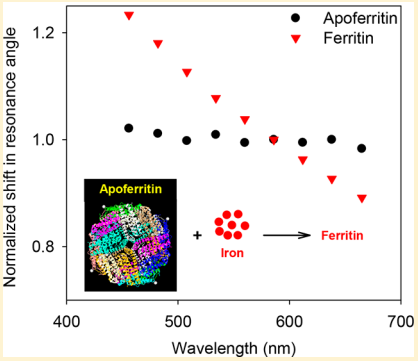

INTRODUCTION

Ferritin serves as the body's primary iron-storage mechanism and has been commonly used as a biomarker for the total body iron content.[1,2] The same protein without any stored iron is called apoferritin. In some conditions such as injury, inflammation, or infection, the ratio of ferritin to apoferritin, and hence the average iron content per protein, may change.[3] The enzyme-linked immunosorbent assay (ELISA), which is the state of the art in clinics, measures combined ferritin and apoferritin concentration because the iron content in the core of the protein does not alter its ability to bind to the corresponding antibody. Iron and protein may be assayed separately using methods such as UV or atomic absorption spectroscopy (AAS) and ELISA, respectively, but the use of two completely different methods adds to the complexity and analysis time of the combined measurement. UV absorption spectroscopy has been shown to be a less reliable method of determining the iron content of ferritin because of structural changes in the iron core of the protein over time.[4] Colorimetric methods for determining iron generally require acidic digestion of the sample followed by reduction to the ferrous state before addition of colorimetric reagents such as *o*-phenanthroline.[5] Methods such as Perls' staining and biochemical assays provide limited information on changes in body's iron content. Previously, the use of magnetic force microscopy has been reported to distinguish ferritin from apoferritin,[6,6] but this method requires a modified atomic force microscope and the samples must be purified and dried and thus cannot be considered a technique suitable for rapid point of care diagnosis and screening.

Label-free methods allow real-time monitoring, offer reduced complexity, and are less tedious to use in comparison to ELISA because they do not require multiple washing steps. Variants of label-free biosensors are optical leaky waveguides (LWs), which are made of low-refractive-index materials such as hydrogels.[7,8] Light in the LWs is confined by phenomena other than total internal reflection (TIR) at either one or both of their interfaces. The simplest structure of such a device is a slab waveguide made from a hydrogel layer sandwiched between a higher refractive index substrate and a lower refractive index cover layer. The confinement mechanism in this structure is TIR at the waveguide−cover layer interface but Fresnel reflection at the waveguide−substrate interface.[9−12] Since the substrate−waveguide interface is leaky, light can be

Received: March 8, 2019
Accepted: May 6, 2019
Published: May 6, 2019

DOI: 10.1021/acs.analchem.9b01231
Anal. Chem. 2019, 91, 7366−7372

coupled into and out of the waveguide through the substrate using a prism. Other researchers have termed these as hydrogel optical waveguides (HOWs)[13−15] because of the material used to fabricate the waveguide.

The resonance angle is determined by the waveguide effective index, which is a function of the real refractive indices of the waveguide and cover (i.e., sample) layers. We have previously shown that the LWs are capable of working over a wide range of wavelengths,[10−12,16] limited only by material absorption or scattering losses at short wavelengths and waveguide cutoff at long wavelengths. Theoretical modeling of a LW consisting of an NBK7 substrate and a 1.5 μm hydrogel layer with a real refractive index 0.01 higher than that of the water cover layer shows that the device can operate from 320 nm (limited by absorption in the BK7 substrate) and 950 nm (limited by cutoff). Thus, LWs allow determining the optical dispersion of the sample species by measuring the resonance angle as a function of wavelength over a broad range. HOWs typically use a layer of gold between the substrate and hydrogel waveguide to permit simultaneous surface plasmon resonance (SPR) and leaky waveguide operation. This limits the operating wavelength range to above 600 nm because the variation of the complex refractive index below this wavelength prevents SPR operation and makes it difficult to visualize the waveguide resonance angle. As discussed later, measurement of dispersion below 600 nm is needed to determine average iron content per protein. Similarly, resonant waveguide gratings[17] and grating-coupled interferometers,[18] although giving high sensitivity to refractive index changes, are strongly dispersive because of the use of grating couplers and high-index waveguides, thus making it difficult to separate the dispersion of the sample from the sensor dispersion.

The porosity of hydrogels is a significant factor in determining the sensitivity of these waveguides as biosensors and arises for two reasons: (1) diffusion of a species into the hydrogel allow it to interact with the fraction of the optical mode confined in the waveguide in addition to the fraction in the evanescent field and (2) capture antibodies for bioassays are immobilized in the entire volume of the hydrogel waveguide, thereby increasing the number of available binding sites for an analyte exposed to the waveguide and thus resulting in an improved sensitivity. Previously, we demonstrated LWs made of agorose, but spin-coated agarose waveguides were largely nonporous to macromolecules and difficult to functionalize to immobilize antibodies.[10,11] A naturally occurring polysaccharide, chitosan, with free amine groups is attractive for the facile immobilization of antibodies. High-refractive-index chitosan waveguides that rely on TIR for light propagation have been reported for sensing relative humidity.[19] Chitosan membranes prepared by casting and rehydration after being dried have been reported to have a pore radius from 1 to 2 nm depending on the degree of cross-linking with glutaraldehyde.[20] These pores are, however, much smaller than the hydrodynamic radius of a majority of proteins,[21,22] and thus such chitosan layers would not be suitable as waveguides to support bioassays. Templating mediated by emulsions or incorporation of nanoparticles followed by leaching has been used to make mesoporous chitosan hydrogels with pore radii between 2 and 50 nm,[23−25] which would be more suitable for protein penetration.

In the work presented here, the feasibility of chitosan films to serve as LWs was investigated for the first time. It was hypothesized and demonstrated that mesoporous chitosan films are obtained by controlling the drying time between spin coating of the film and subsequent rehydration. This involved theoretical modeling along with experimental results relating the effect of film porosity on the measurement sensitivity of species of different molecular weights. We used the chitosan waveguides, for the first time, to determine the optical dispersion of ferritin over the visible wavelength range. More importantly, this is the first report which shows that the optical dispersions of ferritin and apoferritin over the visible wavelength range are significantly different. This difference in the optical dispersions of ferritin and apoferritin was subsequently used to estimate the average iron content of the protein. The average number of iron atoms per molecule of the ferritin used in this study was determined on the basis of the ratio of the resonance angle shifts of ferritin and apoferritin at a selected wavelength. Finally, the resonance angle shifts of ferritin and apoferritin measured using the chitosan waveguide biosensor at two wavelengths was exploited to develop an approach for determining the average iron content of a ferritin sample in a mixture of the two proteins. In summary, we set out to develop a biosensor with a significant potential to enable point of care analysis of ferritin/apoferritin for disease diagnosis and screening.

EXPERIMENTAL SECTION

Chemicals and Materials. Standard microscope glass slides of 1 mm thickness were purchased from VWR (Leicestershire, U.K.). Ethanol, 0.1 M acetic acid, poly(ethylene glycols) (PEGs) of different molecular weights, 4-(2-hydroxyethyl)-1-piperazineethanesulfonic acid (HEPES), reactive blue 4 (RB4), *N*-(3-(dimethylamino)propyl)-*N*′-ethylcarbodiimide hydrochloride (EDC), *N*-hydroxysulfosuccinimide sodium salt (sulfo-NHS), ferritin (F4503), apoferritin (A3660), antiferritin (F6136), and bovine serum albumin (BSA) were bought from Sigma-Aldrich (Gillingham, U.K.). Chitosan (molecular weight 100−300 kDa and 90% deacytelated), glycerol (molecular weight 92), and Decon 90 were purchased from Fisher (Loughborough, U.K.).

Biosensor Fabrication. Glass slides were cut into squares of ∼25.4 mm by 25.4 mm using a diamond scribe and cleaned in Decon 90 solution, water, and ethanol for 30 min after each step in an ultrasonic bath (Ultrawave U300H).

Chitosan was dissolved in 0.1 M acetic acid, and the solution was then spin-coated on a glass slide for 30 s. The concentration of chitosan solution was varied from 0.5% (w/v) to 2% (w/v), and for each solution, the spin speed was varied between 500 and 3000 rpm. The chitosan films were removed from the chuck of the spin coater and allowed to dehydrate for variable times. The films were then rehydrated and cross-linked by immersing in 100 mM HEPES buffer and pH 8.5 buffer without and with 0.016% (v/v) glutaraldehyde for 5 min, respectively. Subsequently, the films were dipped in 0.1 mM RB4 solution in 100 mM HEPES, pH 7.4 for 5 min and washed with the buffer. Finally, the cross-linked and dye-doped chitosan films were stored in 100 mM HEPES buffer, pH 7.4 in the dark until further use.

A 0.5 mg/mL antiferritin solution was prepared in 100 mM HEPES buffer, pH 5.6 containing 2 and 5 mM of EDC and sulfo-NHS, respectively. The reaction was allowed to proceed for 2 h, following which the pH of the solution was increased to 7.4 by adding sodium hydroxide. The activated antibody solution was pumped through a flow cell mounted on the top

DOI: 10.1021/acs.analchem.9b01231
Anal. Chem. 2019, 91, 7366−7372

of the chitosan waveguide and recirculated for 1.5 h to allow antibody immobilization. A 1 mg/mL BSA solution was then used to block free amine groups in the chitosan film. Finally, the response to ferritin and apoferritin was recorded.

Instrumentation. The instrumentation used to test the porosity of hydrogels and performance of waveguide biosensors has been previously described in detail[10−12] and is included inFigure S1 in the Supporting Information. A BK7 equilateral prism (Qioptic Photonics, Denbighshire, U.K.) was used to couple light in and out of the hydrogel waveguide. The light source and the detector were mounted on rails connected to goniometers to allow radial and angular freedom, respectively.

The initial traces of output versus angle of incidence were obtained using a TE-polarized laser (Acculase, RS Components, Northamptonshire, U.K.) with a peak wavelength of 650 nm and a power of 5 mW and a photodiode (OSD100-6, Centronic, Surrey, U.K.).

To obtain spatially and angularly resolved images, the laser was replaced by a 650 nm superluminescent diode (SLD) (EXS210035-02, Exalos AG, Schlieren, Switzerland). The output of the SLD was collimated and subsequently expanded to 25 mm diameter and then passed through a 40 mm focal length cylindrical lens to form a wedge beam to probe the hydrogel waveguide with a range of angles of incidence simultaneously. The SLD was used to reduce speckle in the output, which was imaged using a 6.6 megapixel CMOS camera (PL-B781, Pixelink, Ottowa, Canada). The camera allowed a 7.7 mm wide section of the leaky waveguide to be imaged, which allowed the entire flow channel to be captured in a single frame.

To obtain wavelength and angularly resolved images, the SLD was replaced by a white LED (W57L5111P, Roithner Lasertechnik). An assembly of an achromatic doublet and polarizer was used to obtain a TE-polarized collimated beam. The 40 mm focal length cylindrical lens was then used to obtain a wedge beam. The output of the waveguide was passed through a transmission grating (Thorlabs GT25-03, 300 lines mm^{-1}, blaze angle 17.5°) to disperse the output light and then an achromatic doublet to focus it onto the camera. A slit was used before the grating to ensure that only light which passed through the flowcell region of the device was dispersed and focused onto the camera.

Fluids were pumped through the flow cell using a peristaltic pump (Minipuls 3, Gilson, Bedfordshire, U.K.) at a flow rate of 0.2 mL min^{-1}. The flowcell was CNC machined from 3 mm thick black PMMA, forming a recessed cavity with a 4 mm wide and 0.2 mm deep channel and surrounded by a groove 1 mm wide and 0.75 mm deep in which was mounted an O-ring. The plate was placed on the waveguide biosensor and held in place using a water-cooled fixture maintained at 20 °C.

The refractive index of the solutions was measured using an Abbe refractometer with an accuracy of $\pm 1 \times 10^{-4}$. The UV−vis absorption spectroscopy was performed using a Jenway 6715 UV−vis spectrometer.

RESULTS AND DISCUSSION

Chitosan Waveguides and Their Characterization. The analytical equations governing the LWs have been previously provided.[10] The initial waveguides were fabricated by spin coating 2% (w/v) chitosan solution at 3000 rpm, which was allowed to completely dry out before rehydration. A dip in the reflectivity curve at the resonance angle was observed because of the incorporation of absorption losses introduced by doping the waveguide by RB4. The resonance angle of these waveguides was ∼4.5° higher than the TIR angle, and the width of the resonance dip was ∼5°. Refractive index sensitivity (RIS) of these waveguides was determined by monitoring the shift in the resonance angle for different concentrations of glycerol solutions. The RIS was ∼99.3° RIU^{-1} for glycerol solutions. A comparison of the response of the chitosan waveguide to glycerol and PEG 10k solutions of similar refractive index (see Figure 1) highlights that the two

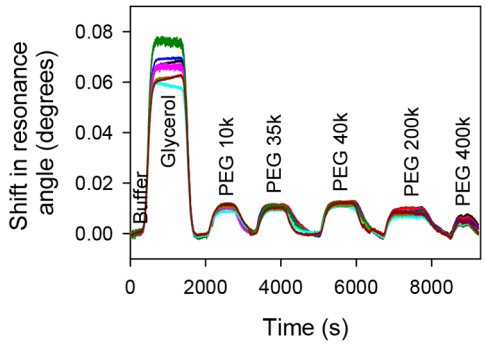

Figure 1. Response of fully dried chitosan waveguide to glycerol and PEG solutions (where different traces represent different positions across the width of the channel).

were significantly different (65.9 ± 5.4 versus 10.8 ± 1.1 millidegrees, respectively). Additionally, the shift in the resonance angle for solutions of PEGs of molecular weight from 10k to 400k was between 7% and 18% of that for the glycerol solution of similar refractive index. This in turn suggested that PEGs with a molecular weight of 10k and higher were unable to diffuse in the waveguide, limiting their interaction to only the evanescent field and hence RIS. This also implies that the waveguide will be nonporous and hence have reduced RIS to biomolecules with molecular weight and geometrical dimensions comparable to those of PEGs. Thus, it was essential to increase the size of the pores in the chitosan waveguides to tens of nanometers: i.e., the typical size of the proteins.[21,22]

The concentration of chitosan solution used to make waveguides was reduced to try to obtain waveguides that are porous to macromolecules. A 1% (w/v) chitosan solution spun at 900 rpm was found to be the lowest concentration of the polysaccharide that resulted in uniform thin films capable of supporting an optical mode. The resulting fully dried films were, however, nonporous. We observed that the films deposited on glass substrates via spin coating were wet on removal from the chuck and their thickness reduced and hence the pores collapsed as they dehydrated. It is likely that the intermolecular forces between the aligned polymer strands after spin coating did not allow these films to swell to their original thickness and regain their pore structure on rehydration. We hypothesized that, by controlling the drying time before rehydration, we could prevent the original pore structure from collapsing and obtain mesoporous chitosan waveguides.

Figure S2a provides the reflectivity curves of the chitosan waveguides of varying drying time before rehydration. Figure S2a clearly illustrates that the resonance angle of the waveguides dehydrated for 1 and 2 min was close to the

DOI: 10.1021/acs.analchem.9b01231
Anal. Chem. 2019, 91, 7366−7372

Table 1. Parameters of Chitosan Waveguides Estimated Using the Transfer-Matrix Program (Where the Cover Refractive Index Is 1.3317)

			RIS (deg RIU^{-1})		
drying time (min)	thickness (μm)	refractive index	nonporous (P = 0)	porous (P = 100)	RIS vs percentage porosity, P
1	2.08	1.3399	22.1	121.8	RIS = 22.06 + 0.9973P
2	1.69	1.3443	21.6	122.6	RIS = 21.56 + 1.0108P
3	1.54	1.3451	25.2	122.6	RIS = 25.20 + 0.9739P
10	1.25	1.3597	16.7	126.3	RIS = 16.69 + 1.0959P

TIR angle (~61.55°) because of their low optical thickness (product of refractive index and geometrical thickness). The film dried for 3 min resulted in a reflectivity dip at the resonance angle with low fwhm, while the film dried for 10 min had the highest resonance angle and fwhm. A surface profiler and white light interferometry were tried to determine the thickness of chitosan films but were unsuitable for characterizing wet films. As discussed previously, dehydrated films do not swell to their original thickness. Thus, combining the thickness of dry chitosan films with swelling studies was unsuitable for determining the thickness of wet films obtained by controlling the drying time before rehydration. Given these challenges, we incorporated a simplex optimization in our transfer matrix program so that the refractive index and thickness of the wet chitosan LWs obtained by controlling the drying time before rehydration could be estimated on the basis of their experimental reflectivity profiles. The results are provided in Table 1.

As shown in Table 1, the thickness of the films decreased exponentially from 2.08 to 1.25 μm as the drying time before rehydration was increased. The refractive index of the films, on the other hand, went up from 1.3399 to 1.3597 as the dehydration time was increased. The theoretical RIS of these waveguides (1) for a nonporous film, i.e. only the evanescent field interacts with the analyte (2) for a fully porous film, i.e. both the evanescent field and optical mode interact with the analyte, and (3) as a function of percentage porosity, P, is also provided in Table 1. While the RIS of nonporous waveguides decreases as the waveguide thickness increases, the RIS of porous waveguides is largely independent of their thickness. Additionally, the percentage porosity, P, of the films is likely to be a function of the molecular weight of analytes. Thus, the RIS of the films will be dependent on the molecular weight of analytes.

Imaging the pore structure of wet chitosan films was challenging using a technique such as SEM that requires dry films along with carbon coating. We were able to visualize the macroporous structure of the freeze-dried chitosan films (results not shown), but the mesoporous structure was damaged as a result of the drying process. Similarly, confocal microscopy required an oil immersion objective to increase the imaging resolution but resulted in drying of the chitosan films. Considering these challenges, diffusion studies were used to determine the porosity of chitosan films. We recorded the shifts in the resonance angle of the LW to assess if species are able to diffuse in the chitosan films.

The films dried for 3 min before rehydration were selected for the remaining work because the dip in reflectivity was easily tracked in real time using a simple, deterministic center of gravity algorithm. The output of the LW captured using a camera shows that the resonance angle, which was evident as a black line in Figure S2b, was uniform over 5 mm wide flow channel. The RIS of the chitosan waveguide for glycerol solutions was 99.3° RIU^{-1}, and its porosity to glycerol solution was estimated to be ~76%. The shift in the resonance angle of the waveguide to glycerol and PEG solutions of different molecular weights is provided in Figure 2 and highlights that the response of the LW varied minimally over the width of the flow channel.

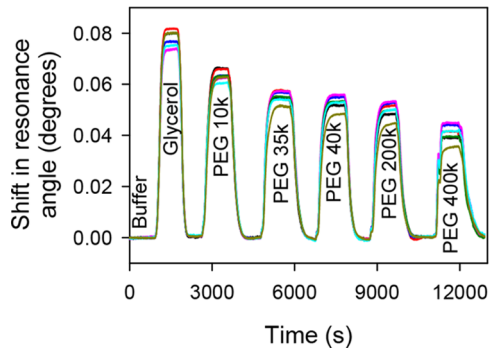

Figure 2. Response of chitosan waveguide dried for 3 min before rehydration (where different traces represent different positions across the width of the channel).

The estimated porosity of the film to different molecular weight analytes is given in Table 2. For example, the difference in the shift in the resonance angle for PEG 10k was only ~19% lower than that of glycerol solution (Figure 2) and the film was estimated to be ~56.9% porous to PEG 10k. This implies that the diameter of ~56.9% of the pores in the chitosan film was at least ~5 nm: i.e., the hydrodynamic diameter of PEG 10k. Similarly, the diameter of ~27.5% of the pores in the chitosan film was at least ~12 nm: i.e., the hydrodynamic diameter of PEG 400k. These results demonstrated the feasibility of producing mesoporous chitosan waveguides by drying the film for 3 min between spin coating and subsequent rehydration.

Chitosan Waveguide Biosensor To Distinguish between Ferritin and Apoferritin. Table 2 shows that $\Delta\theta_R$ value of the fully dried chitosan waveguide to PEG 400k was ~9 times lower than that of the 3 min dried film. Horse spleen apoferritin is a large protein with a molecular weight of ~443 kDa,[26] and the protein is able to accommodate up to 4500 iron atoms in its core.[27] The estimated hydrodynamic diameter of ferritin is ~12 nm,[28] which is comparable to that of PEG 400k. Thus, the waveguide biosensor comprised of the chitosan film dried for 3 min before rehydration was used to study apoferritin and ferritin, because the sensitivity of the partially dried film was expected to be nearly 1 order of magnitude higher than that of the fully dried film.

Figure 3 shows a typical two-dimensional output of a dye-doped chitosan waveguide where the x and y axes represent the wavelength and angle of incidence, respectively. The visualization of the resonance angle was made possible by doping the

DOI: 10.1021/acs.analchem.9b01231
Anal. Chem. 2019, 91, 7366−7372

Table 2. Comparison of Output and Porosity of Chitosan Waveguides to Glycerol and PEG Solutions

	fully dried chitosan waveguide		chitosan waveguide dried for 3 min	
analyte	$\Delta\theta_R$ (millidegrees)	porosity to analyte (%)	$\Delta\theta_R$ (millidegrees)	porosity to analyte (%)
glycerol	65.9 ± 5.4	69.9 ± 5.8	78.1 ± 3.0	76.1 ± 2.9
PEG 10k	10.8 ± 1.1	Nonporous (≤0)	63.5 ± 2.0	56.9 ± 1.8
PEG 35k	10.3 ± 0.8	Nonporous (≤0)	55.2 ± 2.2	46.2 ± 1.8
PEG 40k	11.7 ± 0.7	Nonporous (≤0)	53.1 ± 2.6	43.4 ± 2.1
PEG 200k	8.4 ± 1.2	Nonporous (≤0)	50.0 ± 3.0	39.3 ± 2.4
PEG 400k	4.7 ± 1.3	Nonporous (≤0)	40.9 ± 3.3	27.5 ± 2.2

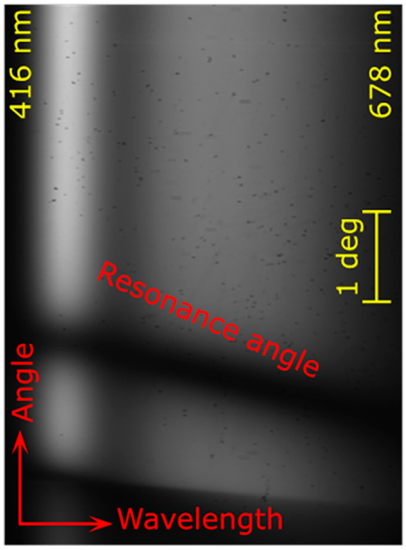

Figure 3. Two-dimensional output of the chitosan waveguide sensor obtained using a white light source and diffraction grating along with camera assembly.

waveguide with RB4 that has a significant absorption over the visible wavelength range. As shown in Figure 3, the resonance angle decreased as the wavelength increased from 416 to 678 nm because the optical thickness of the waveguide decreases at long wavelengths. The intensity of light of wavelength below 450 nm was limited. Thus, the analysis was limited to the wavelength range between 450 and 678 nm. The resonance angle changes with wavelength because of the structural dispersion of the waveguide and the material dispersion of the substrate, waveguide, and aqueous cover layer. Thus, by measurement of the changes in resonance angle with wavelength as protein binds to the waveguide, the additional dispersion introduced by the protein can be determined.

Pankowska and Dobek[29] determined the refractive index increment at 587.6 nm of ferritin containing between 0 and 1500 iron atoms per protein molecule in sodium chloride solutions, showing that it varied between ~1.6 × 10^{-4} and ~2.55 × 10^{-4} g^{-1}, respectively. Since ferritin can contain up to 4500 iron atoms, the extrapolated refractive index increment would be as high as 4.36 × 10^{-4} g^{-1}. The ratio of the ferritin/apoferritin resonance angle shifts from the waveguide at 586 nm was 2.29 (see inset in Figure 4a), which indicates that our ferritin contained 3375 ± 278 iron atoms per protein. This was confirmed by determining the average number of iron atoms per molecule of ferritin by recording the UV−vis absorption spectra of the protein solution. The extinction coefficients of the ferritin solution used in this work were estimated to be 3.596 and 0.557 mL mg^{-1} cm^{-1} at 280 and 450 nm respectively, resulting in an $\varepsilon_{450}/\varepsilon_{280}$ ratio of 0.14. The value reported in the literature for this ratio is 0.116 for ferritin containing 2950 iron atoms per protein.[4] Thus, the average number of iron atoms per molecule of ferritin used in this work was estimated to be 3560 on the basis of UV−vis absorption spectroscopy, which was 5.5% higher than the mean value obtained using the chitosan waveguide biosensor.

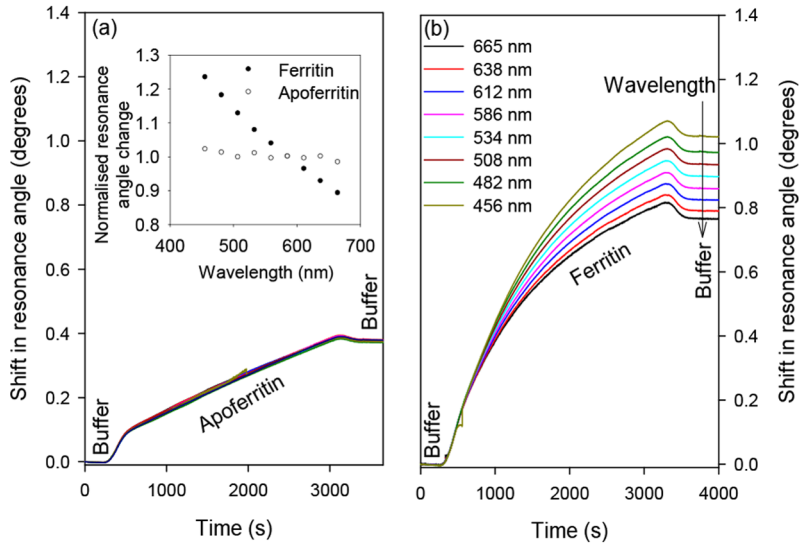

Figure 4. Sensorgrams for (a) apoferritin and (b) ferritin, where the concentration of both proteins was 50 μg/mL and the inset shows the shift in resonance angle (normalized to the shift at 586 nm) after buffer wash for both proteins as a function of wavelength.

DOI: 10.1021/acs.analchem.9b01231
Anal. Chem. 2019, 91, 7366−7372

Figure 4 shows the time response of the waveguide biosensor to (a) apoferritin and (b) ferritin solutions of the same concentration (50 μg/mL) for the same time at wavelengths from 456 to 655 nm. It was observed that the response to apoferritin was considerably lower than that to ferritin, and ferritin showed greater dispersion than apoferritin. Literature studies of the refractive index increment of ferritin and apoferritin have typically been carried out at a single wavelength (usually the sodium D lines);[29] thus, data on the optical dispersion of ferritin are not available.

To determine the average iron content of a sample containing ferritin, different dispersions of ferritin and apoferritin can be used to distinguish the two species and thus determine the average iron content of each ferritin molecule. The slope of the normalized resonance angle shift for apoferritin was -1.29×10^{-4} nm^{-1}, while for ferritin containing 3375 iron atoms per protein the slope was -1.62×10^{-3} nm^{-1}. Thus, the slope m as a function of number of iron atoms per ferritin (N_{Fe}) is given by

$$m = -1.491 \times 10^{-3}\frac{N_{Fe}}{3375} - 1.29 \times 10^{-4}$$
$$= -4.42 \times 10^{-7}N_{Fe} - 1.29 \times 10^{-4}\ \text{nm}^{-1} \quad (1)$$

To obtain the average number of iron atoms per ferritin (N_{Fe}), we inverted eq 1 to obtain

$$N_{Fe} = \frac{m + 1.29 \times 10^{-4}}{-4.22 \times 10^{-7}} \quad (2)$$

Using the normalized resonance angle shift permitted the average number of iron atoms per ferritin (N_{Fe}) to be determined independently of the ferritin concentration, while the absolute resonance angle shift was a measure of total protein concentration.

To demonstrate the selectivity of the method, BSA was introduced on the top of the chitosan waveguide with immobilized antibodies against ferritin/apoferritin. As shown in Figure 5, the shift in the resonance angle of the LW as a result of ~15 μM BSA was ~0.14° and was reduced to 0.07° after a buffer wash of duration of ~500 s. In comparison, the shifts in the resonance angle because of apoferritin and ferritin (both ~0.11 μM) following a similar 500 s buffer wash were ~0.38° and ~0.76−1.03°, respectively. The measurement of ferritin/apoferritin was taken after a buffer wash, which would largely remove any nonspecifically bound sample components. This implies that the response of the chitosan waveguide with immobilized antibodies to nonspecific interactions was minimal and the method is selective toward ferritin/apoferritin.

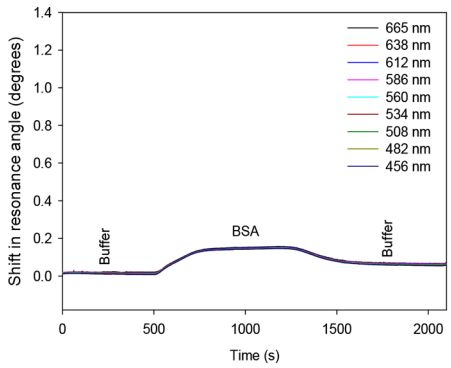

Figure 5. Response of the LW to BSA solution.

CONCLUSIONS

A method of determining the iron content of ferritin has been demonstrated that does not rely on separate determination of iron and protein but instead uses the differences in dispersion between ferritin and apoferritin to perform this measurement in a single step. The use of antibodies in the waveguide provides both selectivity and sensitivity and thus allows interfering species to be removed by washing before measurements are performed. The method is an advance over the the state of the art method, ELISA, because it directly determines the iron content of ferritin. The method of preserving the porosity of chitosan waveguides by rehydration after a suitable time delay post spin-coating improved the measurement sensitivity by a factor of 9. The reported analytical method for determining average iron content of ferritin when it is integrated with suitable sample preparation steps will be highly suitable for point of care applications.

ASSOCIATED CONTENT

Supporting Information

The Supporting Information is available free of charge on the ACS Publications website at DOI: 10.1021/acs.analchem.9b01231.

Schematic of the LW instrumentation, reflectivity curves of the chitosan waveguide dried for different times before rehydration, and 2D output profile of a 3 min dried chitosan LW (PDF)

AUTHOR INFORMATION

Corresponding Author

*R.G.: e-mail, r.gupta@bham.ac.uk; tel, +44 121 414 6119.

ORCID

Ruchi Gupta: 0000-0001-6456-8007

Author Contributions

The manuscript was written through contributions of all authors. All authors have given approval to the final version of the manuscript.

Notes

The authors declare no competing financial interest.

ACKNOWLEDGMENTS

The authors acknowledge funding support from the Engineering and Physical Sciences Research Council (Grants EP/N02074X/1 and EP/N02074X/2). N.A.A. acknowledges the University of Tabuk (Saudi Arabia) for supporting his Ph.D. scholarship.

REFERENCES

(1) Knovich, M. A.; Storey, J. A.; Coffman, L. G.; Torti, S. V.; Torti, F. M. *Blood Rev.* **2009**, *23*, 95−104.
(2) Granick, S. *Chem. Rev.* **1946**, *38*, 379−403.
(3) Kell, D. B.; Pretorius, E. *Metallomics.* **2014**, *6*, 748−773.
(4) May, M. E.; Fish, W. W. *Arch. Biochem. Biophys.* **1978**, *190*, 720−725.
(5) Saywell, L. G.; Cunningham, B. B. *Ind. Eng. Chem., Anal. Ed.* **1937**, *9*, 67−69.
(6) Nocera, T. M.; Zeng, Y. Z.; Agarwal, G. *Nanotechnology* **2014**, *25* (1−5), 461001.
(7) Gupta, R.; Goddard, N. J. *Analyst* **2013**, *138*, 3209−3215.

DOI: 10.1021/acs.analchem.9b01231
Anal. Chem. 2019, 91, 7366−7372

(8) Gupta, R.; Goddard, N. J. *Analyst* **2013**, *138*, 1803−1811.
(9) Hulme, J. P.; Goddard, N. J.; Lu, C. *Sens. Actuators, B* **2011**, *160*, 1508−1513.
(10) Gupta, R.; Goddard, N. J. *Sens. Actuators, B* **2017**, *244*, 549−558.
(11) Gupta, R.; Goddard, N. J. *Analyst* **2017**, *142*, 169−176.
(12) Gupta, R.; Goddard, N. J. *Sens. Actuators, B* **2016**, *237*, 1066−1075.
(13) Wang, Y.; Huang, C. J.; Jonas, U.; Wei, T. X.; Dostalek, J.; Knoll, W. *Biosens. Bioelectron.* **2010**, *25*, 1663−1668.
(14) Zhang, Q. W.; Wang, Y.; Mateescu, A.; Sergelen, K.; Kibrom, A.; Jonas, U.; Wei, T. X.; Dostalek, J. *Talanta* **2013**, *104*, 149−154.
(15) Li, J.; Yu, X.; Herberg, A.; Kuckling, D. *Macromol. Rapid Commun.* **2019**, *40* (7), 1800674.
(16) Gupta, R.; Bastani, B.; Goddard, N. J.; Grieve, B. *Analyst* **2013**, *138*, 307−314.
(17) Paulsen, M.; Jahns, S.; Gerken, M. *Photonics and Nanostructures-Fundamentals and Applications.* **2017**, *26*, 69−79.
(18) Kozma, P.; Hamori, A.; Kurunczi, S.; Cottier, K.; Horvath, R. *Sens. Actuators, B* **2011**, *155*, 446−450.
(19) Voznesenskiy, S. S.; Sergeev, A. A.; Mironenko, A. Y.; Bratskaya, S. Y.; Kulchin, Y. N. *Sens. Actuators, B* **2013**, *188*, 482−487.
(20) Krajewska, B.; Olech, A. *Polym. Gels Networks* **1996**, *4*, 33−43.
(21) La Verde, V.; Dominici, P.; Astegno, A. *Bio-protocol.* **2017**, *7* (8), No. e2230.
(22) Burne, M. J.; Osicka, T. M.; Comper, W. D. *Kidney Int.* **1999**, *55*, 261−270.
(23) Liu, Y. Y.; Tang, J.; Chen, X. Q.; Xin, J. H. *Carbohydr. Res.* **2005**, *340*, 2816−2820.
(24) Huang, G. B.; Yin, Y. B.; Pan, Z.; Chen, M. G.; Zhang, L.; Liu, Y.; Zhang, Y. L.; Gao, J. P. *Biomacromolecules* **2014**, *15*, 4396−4402.
(25) Niamsa, N.; Srisuwan, Y.; Baimark, Y.; Phinyocheep, P.; Kittipoom, S. *Carbohydr. Polym.* **2009**, *78*, 60−65.
(26) Crichton, R. R.; Eason, R.; Barclay, A.; Bryce, C. F. A. *Biochem. J.* **1973**, *131*, 855−857.
(27) Harrison, P. M.; Arosio, P. *Biochim. Biophys. Acta, Bioenerg.* **1996**, *1275*, 161−203.
(28) Crichton, R. R. *Ferritin Metal Bonding in Proteins*; Springer: New York, 1973.
(29) Pankowska, M.; Dobek, A. *J. Chem. Phys.* **2009**, *131* (1−10), 015105.

DOI: 10.1021/acs.analchem.9b01231
Anal. Chem. 2019, 91, 7366−7372